BAMS Article

The Future of Supercells in the United States

Walker S. Ashley, Alex M. Haberlie, and Vittorio A. Gensini

ABSTRACT: A supercell is a distinct type of intense, long-lived thunderstorm that is defined by its quasi-steady, rotating updraft. Supercells are responsible for most damaging hail and deadly tornadoes, causing billions of dollars in losses and hundreds of casualties annually. This research uses high-resolution, convection-permitting climate simulations across 15-yr epochs that span the twenty-first century to assess how supercells may change across the United States. Specifically, the study explores how late-twentieth-century supercell populations compare with their late-twenty-first-century counterparts for two—intermediate and pessimistic—anthropogenic climate change trajectories. An algorithm identifies, segments, and tracks supercells in the simulation output using updraft helicity, which measures the magnitude of corkscrew flow through a storm's updraft and is a common proxy for supercells. Results reveal that supercells will be more frequent and intense in future climates, with robust spatiotemporal shifts in their populations. Supercells are projected to become more numerous in regions of the eastern United States, while decreasing in frequency in portions of the Great Plains. Supercell risk is expected to escalate outside of the traditional severe storm season, with supercells and their perils likely to increase in late winter and early spring months under both emissions scenarios. Conversely, the latter part of the severe storm season may be curtailed, with supercells expected to decrease midsummer through early fall. These results suggest the potential for more significant tornadoes, hail, and extreme rainfall that, when combined with an increasingly vulnerable society, may produce disastrous consequences.

KEYWORDS: Hail; Severe storms; Supercells; Tornadoes; Climate change; Climate models

https://doi.org/10.1175/BAMS-D-22-0027.1
Corresponding author: Walker S. Ashley, washley@niu.edu
Supplemental material: https://doi.org/10.1175/BAMS-D-22-0027.2

In final form 23 September 2022

AFFILIATIONS: Ashley, Haberlie, and Gensini—Department of Earth, Atmosphere, and Environment, Northern Illinois University, DeKalb, Illinois

Deep, moist convection in the atmosphere can take many forms (Doswell 2001). Convective structures that produce severe perils—such as large hail, damaging winds, and tornadoes—are often highly organized and characterized by distinct dynamical flows and features. The most organized deep convective form is the supercell, which was defined by Browning (1964) as a quasi-steady form of cellular convection, with additional dynamical constraints added by others in subsequent decades (cf. Doswell 2001; Markowski and Richardson 2010; Brooks et al. 2019). A supercell is distinguished from ordinary cellular convection by its deep, persistent mesocyclone, which is a storm-embedded, rotating vortex that has a diameter between 2 and 10 km, a vertical depth of at least 2–3 km, temporal continuity of at least 30 min, and vertical vorticity on the order of 10^{-2} s^{-1} or greater. An updraft's interaction with environmental wind shear supports the formation of a supercell's midlevel mesocyclone, which generates a nonhydrostatic vertical pressure gradient, resulting in very intense upward vertical motion. This rotating characteristic is often used to identify supercells operationally and inferred from convection allowing models through proxies such as updraft helicity (UH). While many supercells are discrete, others may be embedded within larger complexes of thunderstorms, or MCSs (cf. Houze 2018). Whether isolated or part of a mixed-mode system, supercells and their quasi-steady, intense, rotating updrafts are thought to produce many of the severe convective storm (SCS) hazards in the extratropical latitudes, including nearly all significant hail (≥50.8 mm diameter) and fatal and/or significant tornadoes (EF2+) in the CONUS (Duda and Gallus 2010; Schoen and Ashley 2011; Smith et al. 2012; Anderson-Frey and Brooks 2019; Ashley et al. 2019). For this reason, supercells and their affiliated hazards have been a focus of a considerable amount of forecasting, observational, field campaign, numerical modeling, climatological, and theoretical research over the last half century (Brooks et al. 2019).

Herein, we are particularly interested in the climatological aspects of supercells, and how anthropogenic climate change (ACC) may affect their frequency, intensity, and spatiotemporal distribution. These supercell attributes will likely be modified in the future as the environmental ingredients supportive of their formation—strong deep-layer shear, robust storm-relative helicity, and sufficient CAPE in a setting with adequate, but not excessive, CIN (Thompson et al. 2012)—are altered due to projected changes in tropospheric kinematics and thermodynamics. Research assessing the impact of ACC on SCS populations has generally employed two approaches (Brooks 2013; Tippett et al. 2015; Allen 2018; Gensini 2021). The first, an implicit—or environmental proxy—approach, uses relatively coarse resolution output from an ensemble of global climate models (GCMs) to assess how the union of instability, shear, and/or forcing ingredients may adjust the occurrence of SCS days or similar metrics in the future (Trapp et al. 2007, 2009; Diffenbaugh et al. 2013; Robinson et al. 2013; Gensini et al. 2014; Seeley and Romps 2015; Brimelow et al. 2017; Hoogewind et al. 2017; Rasmussen et al. 2017; Glazer et al. 2021; Lepore et al. 2021). Results from these implicit efforts suggest that there will be an increase in the number of days supportive of SCSs during the twenty-first century (Brooks 2013; Tippett et al. 2015; Raupach et al. 2021; Gensini 2021). However, more frequent environments supportive of SCSs may not result in more storms due to issues related

to changes in forcing for ascent, reduced boundary layer RH, increased CIN, ingredients juxtaposition, and ultimately, convective initiation and sustenance (Hoogewind et al. 2017; Taszarek et al. 2021; Pilguj et al. 2022).

The second approach uses regional, convection-permitting climate models (RCMs) to explicitly simulate convection and provide more detailed climate information at regional to local scales (Prein et al. 2015; Takayabu et al. 2022; Lucas-Picher et al. 2021). These simulations overcome many of the errors and uncertainties generated by convective parameterization schemes employed by GCMs, but, because of their high spatiotemporal resolution, come with substantial computational expense (Prein et al. 2015; Kendon et al. 2021). Typically, the explicit approach uses a dynamical downscaling technique, where relatively coarse GCM output is used to inform a high-resolution (~4 km horizontal grid spacing), convection-permitting RCM to provide more detailed insight into the future weather peril landscape, though not without some biases (e.g., anomalously warm and dry conditions during boreal summer in the central CONUS; Liu et al. 2016; Haberlie and Ashley 2019; Gensini et al. 2022). Explicit assessments of RCM output remedy aspects of the environmental/implicit approach through the realistic production of convective elements—such as supercells and MCSs—that may be quantitatively identified, tracked, and cataloged using RCM variables so that conclusions may be drawn on how storm populations may change (Rasmussen et al. 2017; Haberlie and Ashley 2019). Broadly, results from the limited dynamical downscaling studies examining climatological scales suggest that SCSs may become more frequent, occur on more days per year, and experience greater variability in occurrence by the end of the twenty-first century (Trapp et al. 2011; Gensini and Mote 2015; Trapp and Hoogewind 2016; Hoogewind et al. 2017; Rasmussen et al. 2017; Trapp et al. 2019; Gensini 2021).

We use output from new, convection-permitting, dynamically downscaled RCM simulations across 15-yr epochs that span the late twentieth and twenty-first centuries to assess how supercellular convection may change in the future. Unlike prior implicit and explicit work on how ACC influences SCS, we identify and track the actual parent storm that produces the most significant and impactful SCS hazards. Like operational forecasting (Kain et al. 2008; Sobash et al. 2011, 2016a,b; Sobash and Kain 2017) and climatological research efforts (Trapp et al. 2011; Robinson et al. 2013; Gensini and Mote 2014; Gropp and Davenport 2021), we use UH from the simulation output as a surrogate for rotating thunderstorms. This variable is frequently used in both deterministic and ensemble forecasting systems to indicate the presence of mesocyclones in model forecasts and has skill at predicting SCSs in operations (Sobash et al. 2011; Potvin and Flora 2015; Sobash et al. 2016a,b; Sobash and Kain 2017). We identify, threshold, segment, and track UH swaths as supercell proxies. Our results reveal how the populations of these long-lived, intense, rotating storms change across the epochs, providing a perspective on how this important storm type may change in the future.

Data and methodology

RCM output. Data used in this research were derived from the simulations generated by Gensini et al. (2022). These RCM simulations employed the advanced research core of the Weather Research and Forecasting Model (WRF-ARW v.4.1.2) in a convection-permitting configuration covering the CONUS, southern Canada, northern Mexico, and adjacent oceans with horizontal grid spacing of 3.75 km and 51 vertical levels. The initial and lateral boundary conditions were forced by bias-corrected GCM data (Bruyère et al. 2014) generated by NCAR's Community Earth System Model (CESM) that participated in phase 5 of the Coupled Model Intercomparison Project (CMIP5). Hereafter, we refer to these RCM simulations as WRF-Bias Corrected CESM (WRF-BCC). We assess three 15-hydrologic-year (1 October–30 September) epochs: a historical period from 1990 to 2005 (HIST) and two future scenarios for the 2085–2100 period. WRF-BCC used a continuous integration approach for each

hydrologic year, with spectral nudging (Miguez-Macho et al. 2004; Gensini et al. 2022) of synoptic features every 6 h, resulting in 45 total simulations. Continuous integration across a hydrologic year is preferred to recreate conditions that require hydrologic memory (Giorgi and Mearns 1999; Chen and Kumar 2002) due to their development over multiple days and months during any given year (Christian et al. 2015; Gensini et al. 2022). The two future scenarios employ the representative concentration pathway 4.5 (RCP4.5) and 8.5 (RCP8.5). RCP4.5 and RCP8.5 are considered intermediate and extreme/pessimistic greenhouse gas concentration trajectories, respectively, and were used by the IPCC in their fifth assessment report (AR5; Moss et al. 2010; IPCC 2014). In offering two RCP perspectives rather than a singular, extreme trajectory provided by previous dynamical downscaling efforts, we do not suggest as to which scenario is more plausible, but, rather, reveal a spectrum of possible outcomes from simulations generated within the context of rational computational expense.

Details on the WRF-BCC configuration and verification of the HIST output against assimilated observations (Daly et al. 1994) are provided in Gensini et al. (2022). The simulation approach used by Gensini et al. (2022) is different from the pseudo–global warming (PGW) approach used by similar research (e.g., Liu et al. 2016; Trapp and Hoogewind 2016). The PGW approach assesses the response of weather variables and climatological metrics to a climate change signal represented through so-called climate change deltas that are constructed using monthly averages of GCM output over decadal or longer periods during the past and future (Trapp et al. 2021). In the simulations employed herein, Gensini et al. (2022) used a version of GCM data (Bruyère et al. 2015) that are regridded and bias corrected using the 1981–2005 ERA-Interim dataset (Dee et al. 2011) following the methods in Bruyère et al. (2014). Bias correction is critical for reducing errors produced by GCMs that may be passed onto an RCM simulation during dynamical downscaling (Christensen et al. 2008), effectively improving the overall simulation performance (Ines and Hansen 2006; Christensen et al. 2008; Gensini et al. 2022). As revealed in Gensini et al. (2022), the WRF-BCC HIST commendably recreated spatial patterns in both temperature and precipitation, though with some regional/seasonal biases as suggested by comparisons to assimilated observational data (e.g., cool-season cold bias east of the Rockies and a warm-season dry bias in the Southeast). In general, the simulations were able to effectively recreate the aggregate historical period of climate when compared to PRISM. Of particular interest for this study, the WRF-BCC reduced warm and dry biases in the Great Plains compared to a prior set of simulations used to assess changes in convective populations (Liu et al. 2016; Rasmussen et al. 2017; Haberlie and Ashley 2019). This reduced bias is important since, as we will illustrate, the Great Plains has the greatest frequency of supercells caused, in part, by thermodynamics driven by surface and/or lower-tropospheric heat and moisture. One additional advantage of the WRF-BCC over a PGW approach is that it accounts for changes in the general circulation and modes of climate variability (cf. chapter 4 in IPCC 2021), which can alter environments and ingredients supportive of SCSs.

Updraft helicity. UH is a diagnostic variable often used to track storm-scale rotation in convection-allowing simulations, and has demonstrated utility in highlighting the potential for rotating storms and affiliated severe weather perils (Sobash et al. 2011; Naylor et al. 2012; Potvin and Flora 2015; Sobash et al. 2016a,b; Sobash and Kain 2017). The variable is computed by taking the vertical integral of vertical vorticity times the vertical velocity in a layer, which, in our case, is 2–5 km AGL [see Kain et al. (2008) for derivation]. This layer samples the lower- to middle levels of a storm, which is where a deep, persistent mesocyclone that defines a supercell is typically anchored. Mesocyclones in this layer—called "midlevel" mesocyclones—are well understood and are generated by the tilting of horizontal vorticity

induced by vertical wind shear into the vertical by way of the tilting term in the vorticity equation (Markowski and Richardson 2010). In this study, we are not sampling low-level (0–2 km AGL) mesocyclones (Sobash et al. 2016b), which tend to have more complicated origins, are often more transient, are poorly simulated by convection allowing models, and may be more directly linked to the production of a single peril—the tornado.

Identifying and tracking supercells. UH data produced by WRF-BCC represent the maximum UH value in the 2–5 km AGL layer for each grid cell over the previous hour ("hourly maximum 2–5 km AGL UH"). We apply a three-dimensional (x, y, and time) object generation approach (Fig. 1) to these UH data to identify, track, label, and catalog UH "swaths" that exhibit hour-to-hour continuity (e.g., Clark et al. 2012). Initially, hourly maximum 2–5 km AGL UH is thresholded to remove regions <75 m^2 s^{-2}; the remaining regions are segmented and assigned unique labels using a 3 × 3 pixel neighborhood. The 75 m^2 s^{-2} threshold is based on research that has used this criterion to delineate and/or forecast supercells and their perils in simulation output at or near the 4 km horizontal grid spacing scale (Clark et al. 2012; Gallo et al. 2016; Sobash et al. 2016a,b; Gagne et al. 2017; Molina et al. 2021; Gropp and Davenport 2021). A consequence of the 75 m^2 s^{-2} threshold is that the procedure does not capture weaker events, and, because we are only considering positive UH values, we capture only those cells that are cyclonic and/or "right moving." Next, spatial buffers of 10 km are generated around each labeled region, and regions are connected in time by checking for spatial overlap between two subsequent hours. Three scenarios can occur: 1) there is no overlap, resulting in track cessation; 2) there is one overlap, resulting in track continuation; or 3) there is more than one overlap, in which case the most similar region (i.e., Hungarian method; Lakshmanan et al. 2013) to the one in the previous time step will be considered the continuation of the track. Matching the most similar regions—determined by finding the smallest difference in area, shape, length, and intensity variables between regions in adjacent hours—is employed to reduce incorrect splits, mergers, initiations, and cessations during storm tracking (Lakshmanan et al. 2013). That said, no tracking method is perfect, and subjective tuning decisions will influence any derived results (Haberlie and Ashley 2018). The tuning decisions made for this work favored retaining robust supercells, while purposely not capturing more transient events. We further enforced this objective by

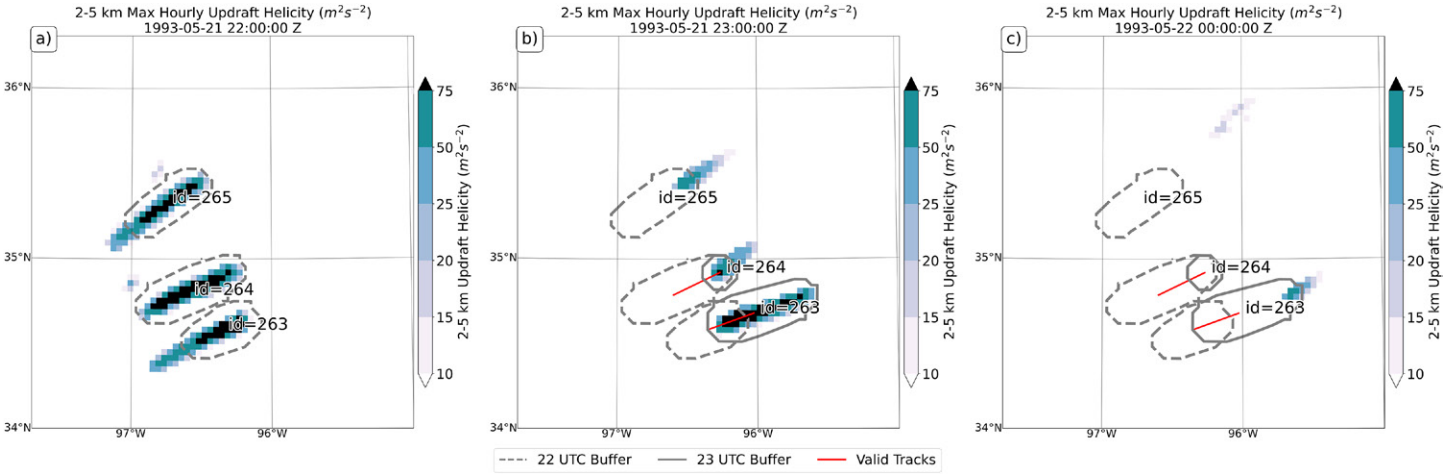

Fig. 1. Demonstration of the method used to segment, track, and catalog supercell in the simulation output. A 10 km buffer (dashed gray line for 2200 UTC and solid gray line for 2300 UTC) is placed around hourly max 2–5 km AGL UH (colored pixels) that exceed 75 m^2 s^{-2}. This hourly "slice" is segmented and assigned a unique label. Next, regions are connected in time by checking for spatial overlap between two subsequent hours, or slices. The valid overlapping slices are then concatenated to form a valid "swath," or footprint to a supercell. Only those tracks lasting at least 2 h are retained for our analysis, which are illustrated here by two unique ID numbers and valid track lines in red.

only keeping those tracks that lasted at least 2 h. The 2 h threshold is based on prior works that have studied the lifespans of mesocyclones in supercells (e.g., Burgess et al. 1982; Wood et al. 1996; Hocker and Basara 2008).

We are interested in assessing all supercell candidates, whether they are isolated or embedded in a mixed-mode system; the latter have received increased attention over the last two decades due to their improved detection and understanding (Ashley et al. 2019). Thus, we did not discriminate for particularly intense, long-lived, and discrete cells using additional data or techniques such as hourly reflectivity maximum, reflectivity isolation buffers around cells, or 3D environmental fields to assess deviant cellular motion from the mean wind. These additional data and methods may be used to identify and track a subtype of supercells that typify the Great Plains in the warm season and are characterized by their intensity and longevity (Bunkers et al. 2006; Gropp and Davenport 2021).

UH is a relatively noisy field in two dimensions after integration due to the centered finite differencing used when solving on the Arakawa C grid that the WRF-ARW employs (Skamarock et al. 2021). The WRF-ARW applies a nine-point smoother before outputting the final UH field. Therefore, it is difficult to obtain extremely high values of UH on the WRF-ARW grid unless the vertical vorticity of a candidate storm has a radius that spans multiple grid points, which may be difficult for some supercells due to their inherent small size relative to larger convective structures. Thus, there is a caveat that the output from the WRF-BCC is conservative when it comes to "true" maximum UH values, or at least in comparison to output that may be produced from other dynamical cores. Nevertheless, each epoch has this possible conservative bias, which should not affect cross-epoch delta comparisons.

The tracking procedure's 2 h criterion and assessment of UH in the 2–5 km layer, rather than, say, 0–2 km layer, likely misses those events that may be characterized by smaller, shallower, transient, and/or weaker mesocyclones and/or mesovortices, especially those supercells affiliated with tropical cyclones (Morin and Parker 2011) and quasi-linear convective systems (QLCSs; Weisman and Trapp 2003; Trapp and Weisman 2003; Schenkman and Xue 2016; Flournoy and Coniglio 2019). Many of these events occur within the Southeast, which may account for the lower-than-expected counts obtained in this region (Smith et al. 2012; Edwards et al. 2012; Sobash and Kain 2017; Ashley et al. 2019). This suggests that 2–5 km UH may not be a reasonable proxy for SCS in some geographies and/or seasons because they may not be characterized by events with strong, midlevel mesocyclones. Further research to remedy this potential issue may need to employ shorter time constraints, evaluate UH in the 0–2 km layer, use a lower threshold of UH, assess 1 km AGL relative vertical vorticity, and/or bias correct 2–5 km UH to diagnose seasonal and regional variations in "weaker" or more transient supercells and their hazard reports.

Given the horizontal grid spacing of 3.75 km in the simulations, we are unable to resolve and quantify how smaller-scale processes (e.g., boundary layer turbulence; Markowski 2020) and any affiliated changes due to ACC in those processes may affect supercell character. While such processes may be important for the perils that supercells can generate, we believe that they are less important for understanding the overall climatological characteristics of supercells, which is our focus in this study.

Finally, we provide statistical significance tests ($p < 0.05$; Mann–Whitney U test) in many of our supercell count and environmental analyses, but caution that confidence in statistically significant differences is relatively low due to 1) small sample sizes ($n = 15$) and 2) in the case of supercell events, we are examining extreme event data that are highly variable and may be influenced by singular events and/or outlier periods of (in)activity. Significance tests use 15 years (or seasons) of data (counts, means, etc.) for HIST and respective FUTR epochs.

Results

Cumulative updraft helicity. Initially, we evaluate the frequency of the full spectrum of hourly maximum 2–5 km AGL UH thresholds for the central and eastern CONUS (Fig. 2). Generally, a separation in total grid cell counts by UH magnitude for the three epochs does not occur until a threshold of ~150 m^2 s^{-2} is exceeded, with the overall count ceiling much

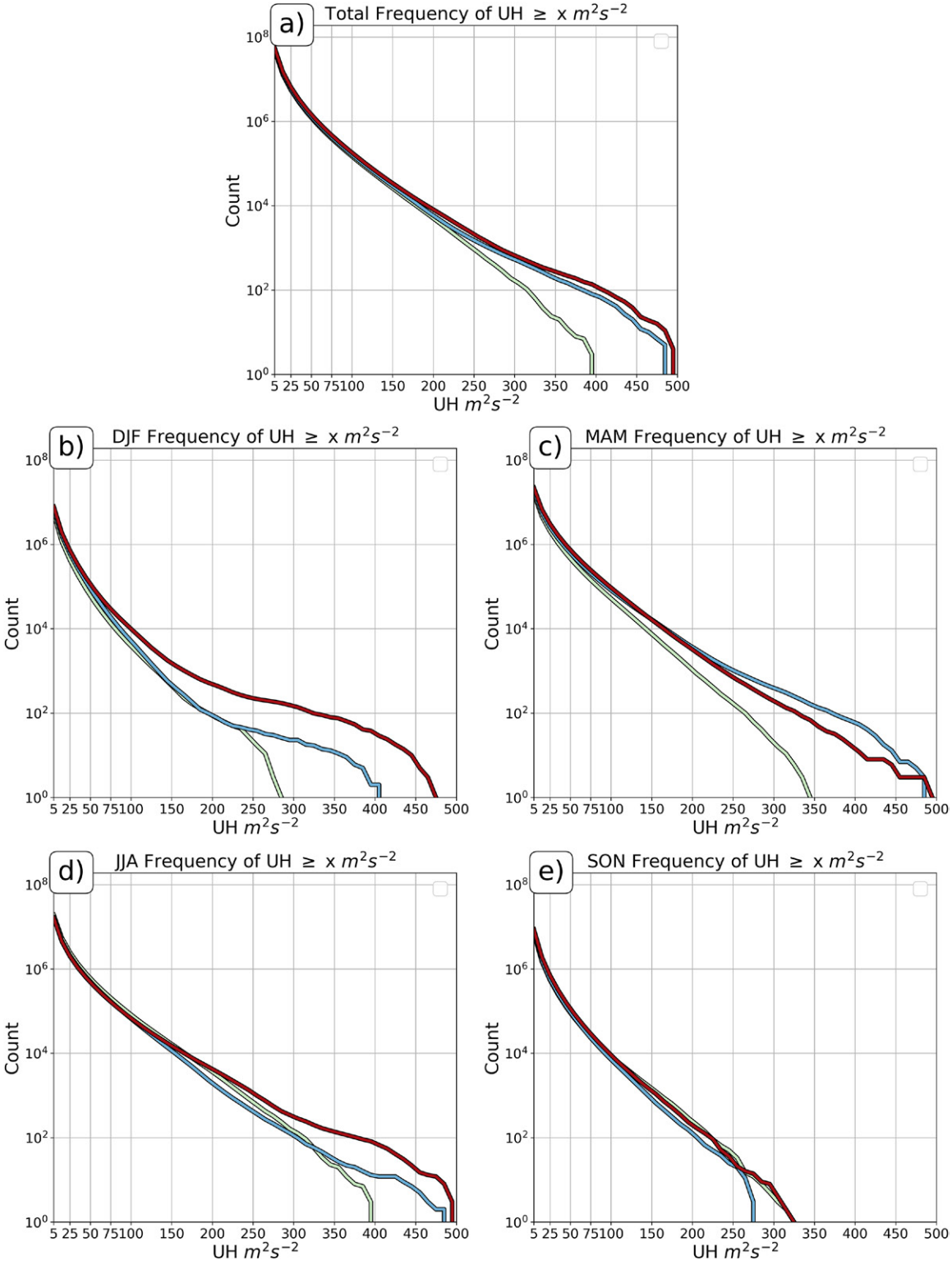

Fig. 2. The frequency (*y* axis) of 3.75 km grid cells of hourly maximum 2–5 km AGL UH that meet certain thresholds (*x* axis) for the three epochs (colored lines) for (a) annual, (b) winter (DJF), (c) spring (MAM), (d) summer (JJA), and (e) fall (SON) for the central CONUS (cf. Fig. 3a dashed rectangle for domain).

greater for particularly intense UH (≥200 m^2 s^{-2}) grid cells in the projections for the end of the twenty-first century. While there is much separation in intense thresholded grid cell counts between the HIST and FUTR epochs, there is little difference in annual counts between the FUTR epochs. This lack of difference between FUTR epochs is largely due to a seasonal discrepancy in grid cell counts, particularly in the winter, spring, and summer. Intense threshold counts in the FUTR4.5 epoch exceed the FUTR8.5 epoch in the spring, whereas the FUTR8.5 exceeds the FUTR4.5 counts in the winter and summer. Despite seasonal differences, it is projected that particularly intense storm rotation will be more prevalent in a future climate under both intermediate and pessimistic greenhouse gas concentration trajectories. The strong correlation between UH and SCS perils (Clark et al. 2013; Sobash et al. 2016a; Gagne et al. 2017) suggests that this would lead to more hazards in the future, including significant tornado and hail events.

Spatial and temporal climatology. Spatially, the WRF-BCC does an admirable job of representing the probable climatology of supercells (Fig. 3a; Gensini and Ashley 2011; Smith et al. 2012; Taszarek et al. 2020; Davenport 2021), though an extensive climatology of CONUS supercells based on observed data has not been generated to date. As discussed in the methods, we are likely undercounting supercells that tend to be shallow or transient as inferred by environmental proxies and/or SCS peril climatologies (Sherburn and Parker 2014; Davis and Parker 2014; Childs et al. 2018; Ashley et al. 2019), which may lead to climatological unrepresentativeness—depending on how one defines a supercell—in parts of the Southeast, Ohio valley, and mid-Atlantic.

Deltas, or changes, between the HIST and FUTR epochs follow a similar pattern with increased supercell tracks found east of 95°W and, generally, decreases in the Great Plains (Rossum and Lavin 2000), or west of Interstate 35 (Figs. 3b–e). The greatest positive track change is found between HIST and FUTR8.5, with increased events maximizing in north Texas and the Ark-La-Tex and Ozark Plateau regions with broad increases found elsewhere in the mid-South and western Great Lakes. The net positive pattern is similar in the HIST and FUTR4.5 delta but is more muted in the eastern Arkansas River valley, with delta maxima displaced toward the mid-South and central Gulf Coast. The FUTR increases in the eastern Arkansas and lower Mississippi River valleys are driven by rising seasonal numbers, particularly in the spring and, to a lesser extent, the winter (Fig. ES1 in the online supplemental material; https://doi.org/10.1175/BAMS-D-22-0027.2). Future decreases in both delta assessments are concentrated in portions of the Great Plains, from south Texas to South Dakota, with a notable reduction found from the High Plains of Colorado through the middle Missouri valley (Fig. 3). Contrary to the South, these changes are caused by reduced supercell counts across wide expanses of the central CONUS during the summer (Fig. ES1).

Like UH grid cell counts, a dichotomy is found in the HIST and FUTR deltas, with robust and, in some cases, significant, supercell count and areal footprint increases found in the late-twenty-first-century epochs for February, March, and April and declines in June, July, and September (Fig. 4; Table 1; Table ES1 and Figs. ES2–ES5). Thus, supercells are projected to be more prevalent in the early severe weather season, while declining in frequency in the late season. Considering the seasonality of SCSs and their environments, this suggests that the early-season supercells will affect regions of the southern tier of the CONUS, which is an area that is particularly vulnerable to supercell perils (Ashley 2007; Ashley et al. 2008; Ashley and Strader 2016; Strader et al. 2017a,b, 2021). Meanwhile, late season events, which typify the High Plains and northern plains, will be less frequent, likely a consequence of the increasing CIN that is expected across that geography (Hoogewind et al. 2017; Rasmussen et al. 2017; cf. "Environmental ingredients" section).

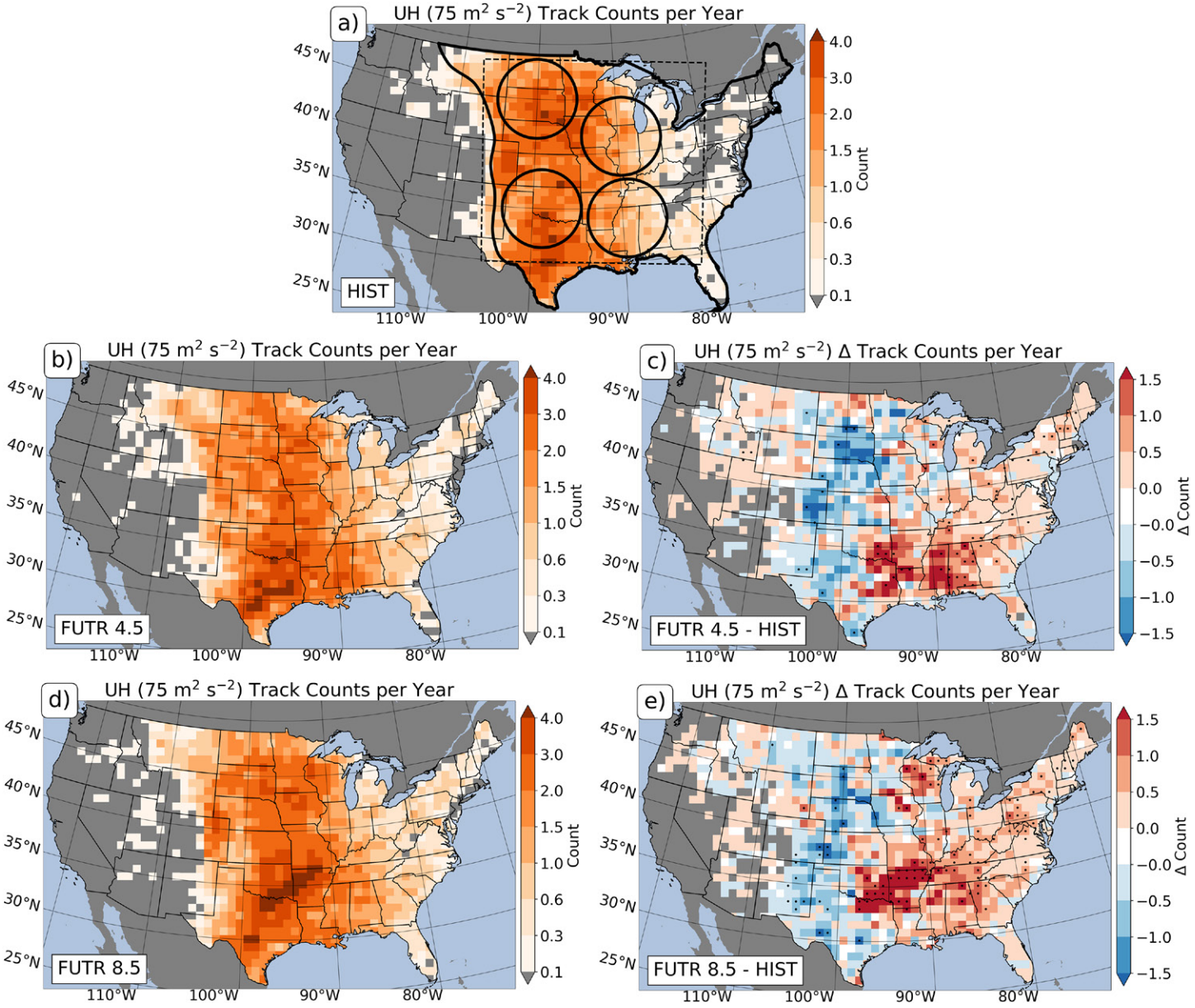

Fig. 3. Mean annual supercell track counts on an 80 km grid for the three simulation epochs: (a) HIST, (b) FUTR4.5, and (d) FUTR8.5. (c),(e) The mean annual supercell count track differences, or deltas, between FUTR4.5 and HIST and between FUTR8.5 and HIST, respectively. (a) illustrates domains assessed, which include east CONUS (solid outline east of Continental Divide); central CONUS signified (dashed rectangle); and subregions centered in the northern plains, southern plains, Midwest, and mid-South (circles). Stippling denotes a significant ($p < 0.05$; Mann–Whitney *U* test) difference between HIST and FUTR8.5.

Additional annual metrics—supercell hours, total accumulation of UH values for all supercells, and cumulative spatial extent of UH within supercells—follow similar trends as those found in annual supercell track counts (Fig. 5; Table 1; Table ES1 and Figs. ES2–ES5), with overlap in the interquartile range, but with general increases found for future epochs, though with mixed results when testing for statistical significance. The annual UH track accumulation, which is effectively the sum of all UH pixel values in all qualifying supercells swaths, has less overlap in the interquartile range compared to track counts and hours, with a notable increase—though, not statistically significant—in central tendencies. This jump in future total track accumulation suggests the potential for not only more supercells, but longer-lived, or more intense ones, when they do occur. The most striking differences between HIST and FUTR epochs were found in the annual UH cumulative areal extents for strong (≥100 m^2 s^{-2}) and intense (≥200 m^2 s^{-2}) thresholds. Track accumulation extents at the strong threshold have a mean (median) increase of

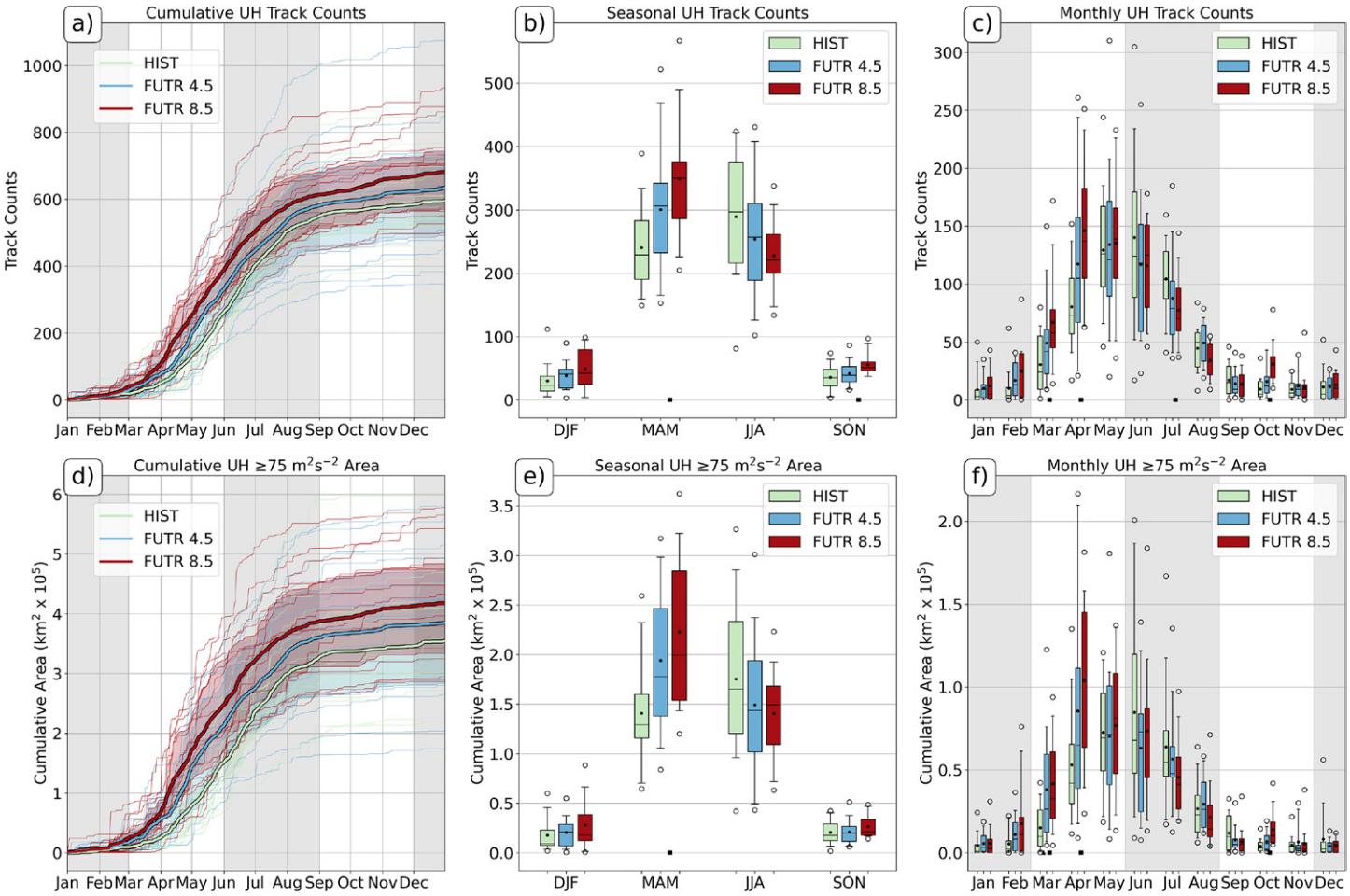

Fig. 4. (a) Annual cumulative frequency of supercell counts for the three epochs for the eastern CONUS (see Fig. 3a for domain), as well as (b) seasonal supercell counts and (c) monthly supercell counts for the three epochs illustrated using box-and-whisker diagrams. (d)–(f) As in (a)–(c), but for cumulative areal footprint of supercells. In (a) and (d), means are denoted by thicker lines with the 25th- and 75th-percentile bounds provided in epoch-respective color shading. For (b) and (c) and (e) and (f), means are denoted by black dots, medians by the black lines, the boxes represent the interquartile range, the whiskers illustrate the 5th and 95th percentiles, and the clear circles denote outliers. A triangle (square) denotes a significant ($p < 0.05$; Mann–Whitney *U* test) difference between HIST and FUTR4.5 (FUTR8.5).

9.3% (28.7%) from HIST to FUTR4.5 and 19.2% (26.8%) from HIST to FUTR8.5, whereas intense threshold accumulation extents have a mean (median) increase of 25.8% (11.9%) from HIST to FUTR4.5 and 60.2% (92.1%) from HIST to FUTR8.5. These projected FUTR threshold areal extent increases are concerning as these extreme mesocyclones are more likely to produce perils that have societal impacts.

Despite net positive percent changes in annual mean and median values for all supercell metrics from HIST to FUTR epochs (Table 1), seasonal trends during the typical peak of SCS season are varied (Table ES1). Much like supercell counts, supercell hours, spatial extents, and cumulative UH metrics all have dramatic increases in the winter and early spring for both FUTR epochs, while stable to decreasing values for summer. This, again, suggests a more robust earlier SCS season in the future due to increased supercell populations and/or magnitudes, with reduced presence of supercells and their perils during June–September. The most dramatic percent increases in supercells metrics from HIST to FUTR are found during the winter and early spring, with, in some cases, a near doubling of monthly metrics, particularly for the FUTR8.5 delta. Conversely, many of the June–September supercell metrics decline, on average, from 10% to 30% in the FUTR. Despite the notable increases found in the cool and spring transition seasons, we acknowledge that our data and methods do not fully account for the potential changes that may occur since events during this period have a

Table 1. Measures of central tendency for eastern CONUS annual supercell metrics illustrated in Fig. 5. The two right columns include positive percentage changes in central tendencies for FUTR vs HIST epochs. The only significant ($p < 0.05$; Mann–Whitney U test) difference is in the 200 $m^2 s^{-2}$ threshold at RCP8.5.

				Relative change (%)	Relative change (%)
	HIST	FUTR4.5	FUTR8.5	HIST vs FUTR4.5	HIST vs FUTR8.5
		Supercell counts			
Mean	595	634	682	6.6	14.5
Median	553	642	702	16.1	26.9
		Supercell hours (h)			
Mean	1,474	1,547	1,645	5.0	11.6
Median	1,375	1,542	1,712	12.1	24.5
		Supercell swath UH accumulation ($m^2 s^{-2} \times 10^5$)			
Mean	26.3	28.7	31.3	9.3	19.2
Median	24.6	30.1	31.7	12.1	28.9
		Cumulative areal extent UH ≥ 75 $m^2 s^{-2}$ ($km^2 \times 10^5$)			
Mean	354,274	384,985	417,736	8.7	17.9
Median	336,783	405,211	421,116	20.3	25.0
		Cumulative areal extent UH ≥ 100 $m^2 s^{-2}$ ($km^2 \times 10^5$)			
Mean	150,120	163,943	179,756	9.2	19.7
Median	135,703	174,698	172,069	28.7	26.8
		Cumulative areal extent UH ≥ 200 $m^2 s^{-2}$ ($km^2 \times 10^5$)			
Mean	5,208	6,553	8,345	25.8	60.2
Median	4,627	5,175	8,888	11.9	92.1

higher likelihood to be supercells, sometimes embedded in QLCS structures, that tend to be smaller, shallower, transient, and/or weaker due to a weakness in environmental ingredients such as moisture and instability (Smith et al. 2012; Sherburn and Parker 2014; Ashley et al. 2019). Thus, the net increase in the number of supercells, their magnitudes, and their perils may be even more substantial during future early SCS seasons. May, which is typically the CONUS peak climatology for supercell-related perils of hail and tornadoes, is the only month during the climatologically active part of the season without substantial changes in supercell metrics. This may be due to the environmental "goldilocks" character of this month, when ingredients of SCSs have, and will likely continue to, comingle frequently and at just the proper amounts, while months on either side of May deal with dichotomous changes in their respective overlap of important ingredients (Hua and Anderson-Frey 2022).

A regional perspective on the differences in supercell counts between epochs reinforces the narrative of "more early, less later," with the eastern CONUS, northern and southern plains, and Midwest all having a notable increase in counts for their respective early severe weather seasons, with decreases in the latter half of the season (Fig. 6). The mid-South domain has notable FUTR positive increases restricted to February, March, and April, with negligible change in all other months.

Environmental ingredients. The patterns found in the supercell population analyses are a consequence of fundamental SCS environmental ingredients and their expected changes in the future (Diffenbaugh et al. 2013; Seeley and Romps 2015; Hoogewind et al. 2017; Glazer et al. 2021; Lepore et al. 2021). Specific to our simulations, WRF-BCC reveals increasing instability throughout the central and east CONUS in the FUTR epochs, with very large, and significant, changes in annual (Figs. 7a–c) and seasonal MUCAPE (Figs. ES6–ES9a–c; cf. Fig. 4 in Haberlie et al. 2022) found east of the Mississippi River,

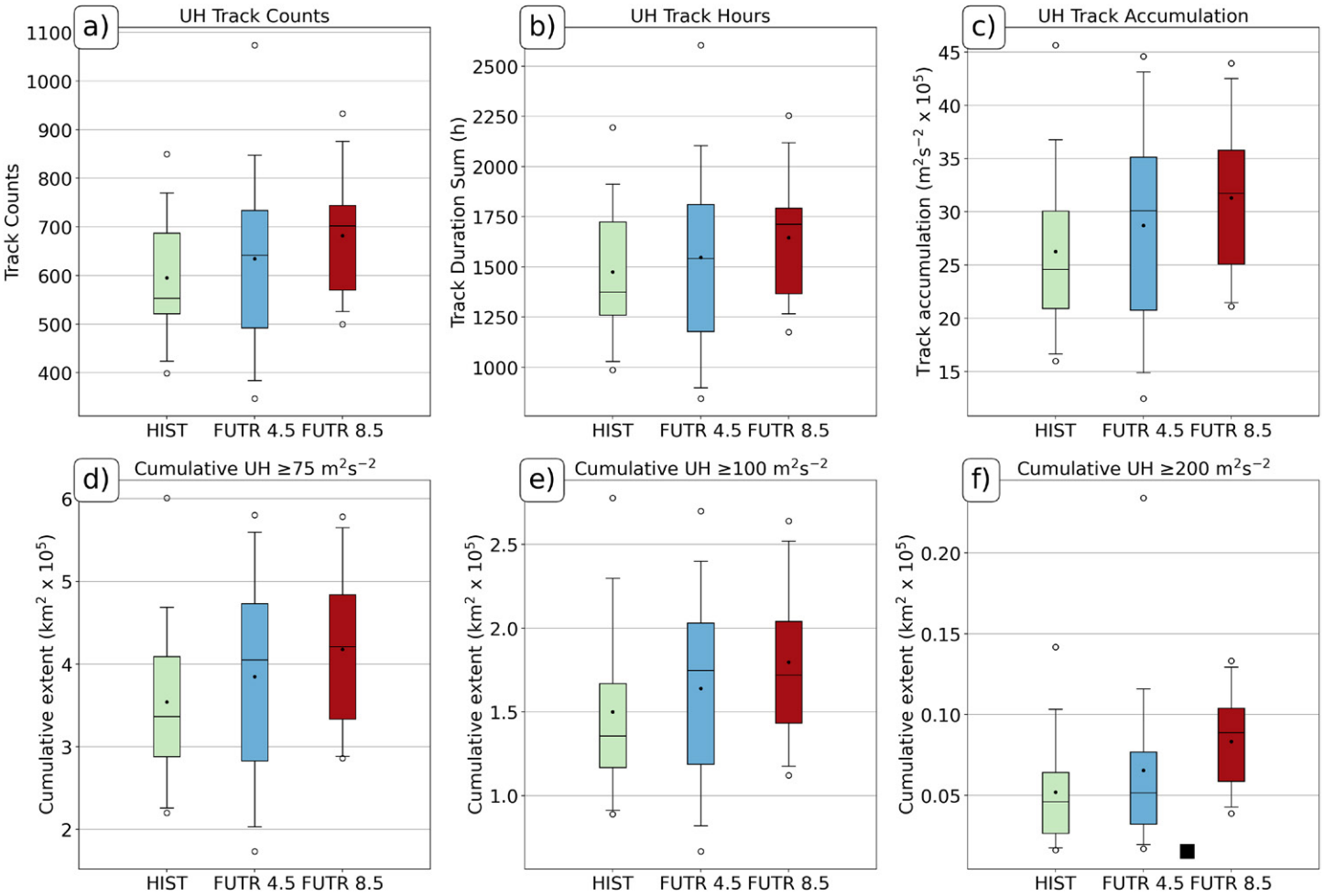

Fig. 5. Box-and-whisker plots illustrating annual eastern CONUS (a) supercell counts, (b) sum of supercell track hours, or count of hourly supercell slices, (c) UH accumulation, or the sum of all UH values in all qualifying supercell slices, and (d)–(f) areal track accumulation extents for 75 m^2 s^{-2}, 100 m^2 s^{-2} (intense), and 200 m^2 s^{-2} (extreme) thresholds, respectively. Box-and-whisker distributions and central tendencies as in Fig. 4. A triangle (square) denotes a significant ($p < 0.05$; Mann–Whitney *U* test) difference between HIST and FUTR4.5 (FUTR8.5).

particularly in the HIST-FUTR8.5 delta during the warm season. Conversely, MUCIN increases throughout the central CONUS (Figs. 7d–f), with maximum MUCIN deltas between the HIST and FUTR epochs found across the Great Plains during the warm season (Figs. ES6–ES9d–f; cf. Fig. 4 in Haberlie et al. 2022), consistent with that found in recent research using RCP8.5 (Hoogewind et al. 2017; Rasmussen et al. 2017). This suggests that, although MUCAPE may increase in the future, some of this instability may not be realized due to increasingly capped environments that will not support convection initiation and/or sustenance (Hoogewind et al. 2017; Rasmussen et al. 2017), especially near and just east of the elevated-mixed-layer source regions along the western fringes of the supercell climatological maximum.

While CAPE is a fundamental ingredient for thunderstorms, it is not the only environmental constituent required for SCS. Deep-layer vertical wind shear, which is the atmospheric condition that promotes organization in storms like supercells, generally decreases across the study domain in the future on an annual basis (Figs. 7g–i), though these changes are more complex when assessed seasonally (Figs. ES6–ES9g–i). For instance, there is a notable increase in shear across regions that are frequented by supercells during the FUTR8.5 spring. That said, it is the *overlap* of fundamental ingredients that promotes supercells and other forms of SCS. A well-known composite parameter that may be used to gauge the juxtaposition of CAPE and various qualities of shear [e.g., 0–6 km bulk wind shear and 0–3 km storm-relative helicity

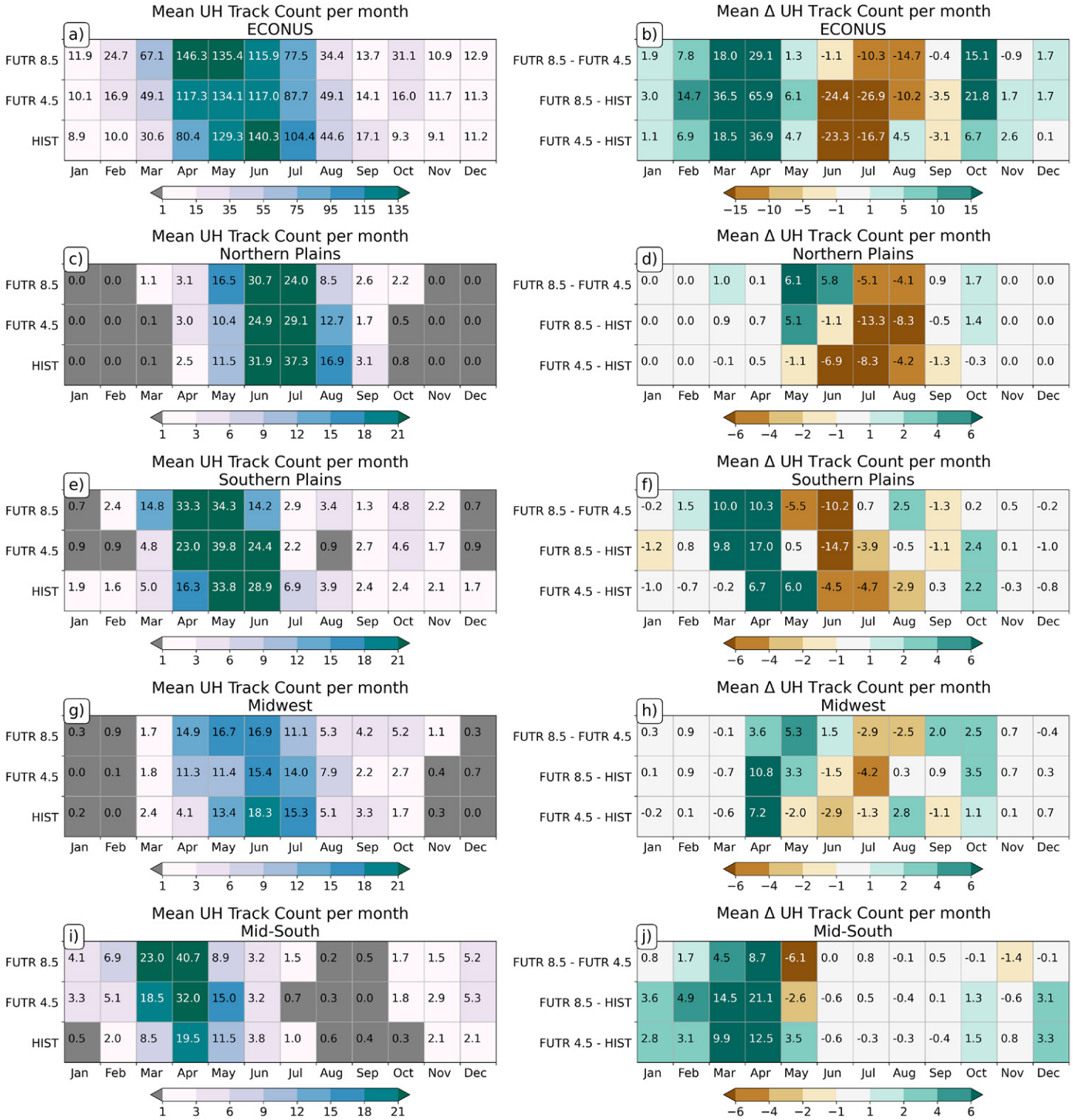

Fig. 6. Chiclet charts of the mean annual UH counts per month for the three simulation epochs for the (a) eastern CONUS and (c),(e),(g),(i) subregional domains illustrated in Fig. 3a. (b),(d),(f),(h),(j) Mean annual monthly count differences, or deltas, between epochs labeled on *y* axis.

using the Bunkers et al. (2000) storm motion estimate] supportive of rotating storms is the supercell composite parameter (SCP; Thompson et al. 2003). This parameter is used frequently in forecast and climatological applications to assess environments supportive of supercells and their perils (e.g., Gensini and Tippett 2019; Krocak et al. 2021; Taszarek et al. 2021). Only SCP deltas between HIST and FUTR8.5 are examined herein, as not all variables needed to calculate SCP were retained for the FUTR4.5 simulations due to data storage constraints.

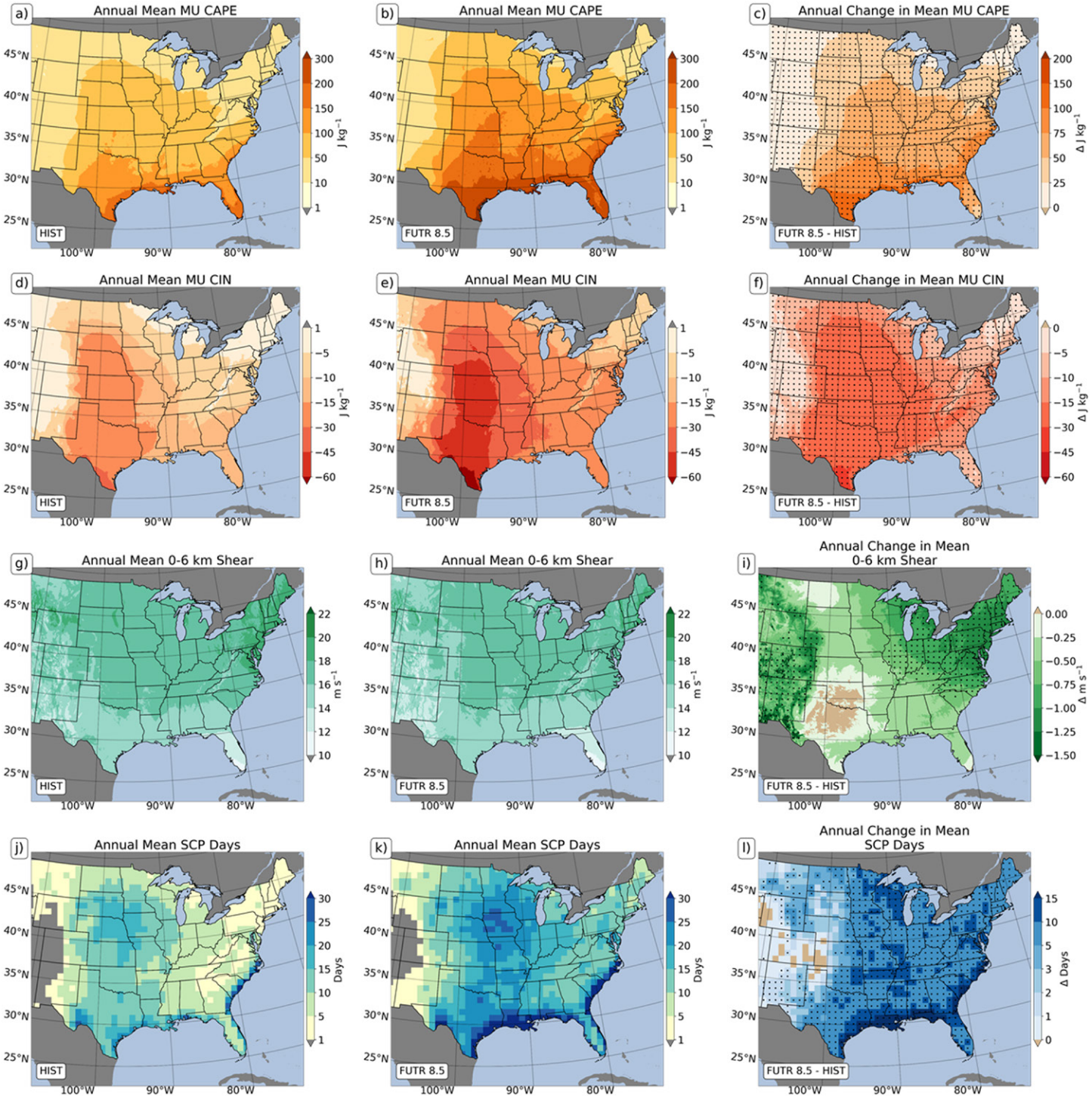

Fig. 7. Mean annual hourly MUCAPE for (a) HIST, (b) FUTR8.5, and (c) FUTR8.5 vs HIST; MUCIN for (d) HIST, (e) FUTR8.5, and (f) FUTR8.5 vs HIST; and 0–6 km shear for (g) HIST, (h) FUTR8.5, and (i) FUTR8.5 vs HIST. Mean annual supercell composite parameter (SCP) days for (j) HIST, (k) FUTR8.5, and (l) FUTR8.5 vs HIST. An SCP day is defined as a day when at least one hourly SCP value at a grid point was greater than or equal to 1. Stippling denotes a significant ($p < 0.05$; Mann–Whitney *U* test) difference between HIST and FUTR8.5.

Except for a small portion of the central High Plains, most of the study domain experiences a significant increase in the number of mean SCP days in FUTR8.5, with greatest increases in the Midwest, through the Ozarks, and equatorward to the Gulf Coast (Figs. 7j–l). The most notable seasonal increases in SCP days in the FUTR8.5 are clustered in the spring across the south-central CONUS and mid-South, and, during the summer, across the Great Lakes, Northeast, and East Coast. FUTR8.5 seasonal declines in SCP days are prominent in portions of the

Great Plains during JJA, which is also the region and season that is expected to experience an increasingly hostile environment for convective initiation and sustenance due to robust increases in MUCIN. Generally, this macroscale analysis of ingredients suggests there will be a reduced number of future environments supportive of supercells in portions of the Great Plains, with broad increases found east of 95°W. Changes in the spatiotemporal trends in the environmental analysis are similar to the shifts in the WRF-BCC supercell populations, illustrating the importance of overlapping SCS ingredients and how any modification in this overlap in the future may result in change to the overall SCS climatology. This will have consequences for not only SCS peril production, but an important hydrologic input in many regions of the CONUS (Smith et al. 2001; Hitchens and Brooks 2013).

Diurnal cycle. There is little change in the diurnal cycle of supercell counts as measured by their initiation, cessation, and total hourly counts between the FUTR and HIST epochs in the eastern CONUS domain (Fig. 8). However, regionally, the mid-South and northern plains have noteworthy shifts in future supercell populations over the course of the day.

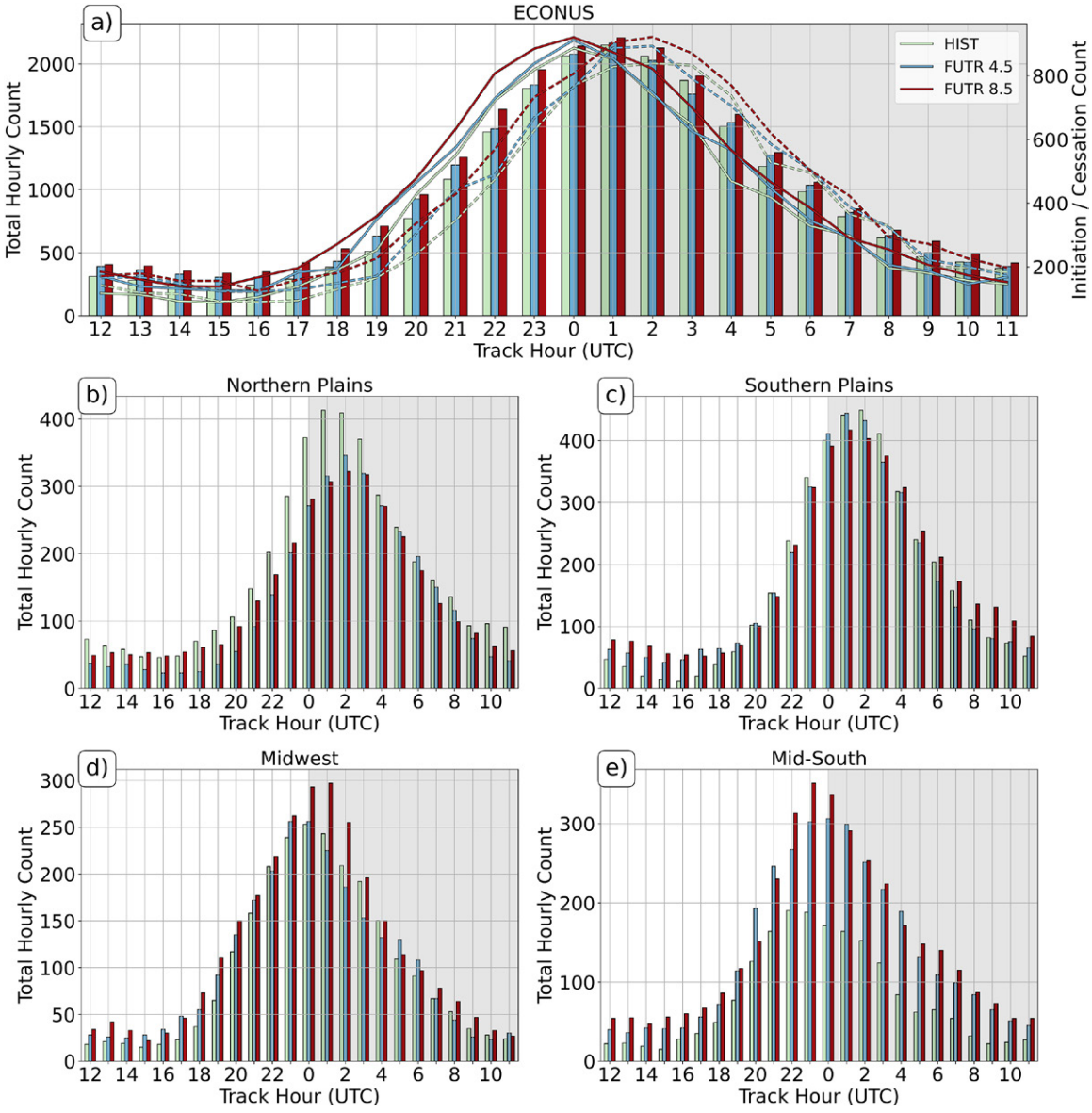

Fig. 8. Total hourly supercell counts (bars) for the three simulation epochs for (a) eastern CONUS and (b)–(e) subregional domains illustrated in Fig. 3a. The plot in (a) also contains initiation (lines) and cessation (dashed lines) for the eastern CONUS domain.

Of particular concern is the mid-South. As discussed, supercells in the mid-South are projected to become more frequent, with the diurnal analyses showing large increases in supercell occurrences in both FUTR scenarios for the midafternoon through overnight hours. Similarly, the cumulative supercell extent, or footprint, increases by roughly 70% in both FUTR scenarios during the evening and overnight period (not shown) for the mid-South. This increasing supercell frequency and footprint extent will be clustered in the winter and early spring, when daylength is at a minimum; this may result in an enhanced threat of nocturnal tornadoes (Duda and Gallus 2010; Schoen and Ashley 2011; Smith et al. 2012; Krocak and Brooks 2018; Anderson-Frey and Brooks 2019; Ashley et al. 2019). Evening and overnight tornadoes are an impediment to warning efficacy (Mason et al. 2018) and are up to 2.5 times as deadly as their daytime counterparts (Ashley et al. 2008; Strader et al. 2022), which suggests an increasing likelihood of future deadly events in this region unless mitigation efforts are improved. Conversely, supercells in the northern plains are projected to decrease, with most of that decline occurring during the afternoon and evening hours during a season when daylength is near maximum, which may reduce the overall societal threat in the region (Ashley et al. 2008; Strader et al. 2022). The Midwest has mixed diurnal results, with a large uptick in hourly counts during the evening hours for FUTR8.5, but little difference between the FUTR4.5 and HIST.

Conclusions

Our understanding of how ACC will affect SCSs is in its infancy (Kunkel et al. 2013; NAS 2016). Continued research employing both implicit and explicit methods will be required to increase our knowledge of how ACC may change SCS frequency, intensity, and location (Gensini 2021). Herein, we used an explicit approach, employing UH generated from both historical and future dynamically downscaled simulations as a proxy for supercells to evaluate how this important peril producer may change in the future. We offered two end-of-century perspectives, employing intermediate and pessimistic greenhouse gas concentration trajectories to reveal prospects on the future of supercells and their hazards in the CONUS.

Projections from WRF-BCC suggest that supercells will become more frequent in the twenty-first century in regions of the eastern CONUS, while decreasing in frequency in portions of the Great Plains. This mimics a recent observed trend in tornado environments and reports (Gensini and Brooks 2018; Taszarek et al. 2021), which is conflating with elevated—and, projected to escalate—exposure and vulnerability in these increasingly risky areas. With supercell risk, human and built-environment exposure, and socioeconomic vulnerabilities projected to rise in the Ozarks, mid-South, and Tennessee valley, the likelihood for more impactful tornado events in these regions is certain for the twenty-first century (Ashley and Strader 2016; Strader et al. 2017a,b, 2021). Supercell risk is likely to escalate outside of the typical SCS season, with these storms and attendant perils projected to increase in late winter and early spring months under both intermediate and pessimistic trajectories. Conversely, the latter part of the SCS season may be curtailed, with supercell populations projected to decrease in June through September. Events during the summer and early fall typically affect regions that have relatively low exposure and vulnerability (Ashley 2007; Ashley et al. 2008; Ashley and Strader 2016), which suggests disaster potential in these areas may remain relatively curbed. Of particular concern for future impacts is the growing likelihood of supercells to contain more strong and intense UH-defined mesocyclones, which correlates with the production of SCS perils such as significant tornadoes and hail (Clark et al. 2013; Sobash et al. 2016a; Gagne et al. 2017).

The projected spatiotemporal changes in supercells are driven by likely changes in the ingredients required for these storms and other SCS morphologies (cf. summaries by

Brooks 2013; Tippett et al. 2015; Allen 2018; Raupach et al. 2021; Gensini 2021). While not the focus of this study, the background states of increasing moisture and instability in a warming climate, particularly during the early season, will lead to more supportive environments, and potentially more robust updraft formation, in the future (Trapp et al. 2007; Diffenbaugh et al. 2013; Marion and Trapp 2019). The latter part of SCS season is characterized by a more hostile capping environment, with CIN expected to increase across regions where supercells climatologically roam (Hoogewind et al. 2017; Trapp et al. 2019; Taszarek et al. 2021). Our projections reveal a decrease in supercells under both RCPs assessed across broad swaths of the Great Plains west of Interstate 35, which, on one hand, could lessen the threat for SCS perils such as tornadoes and hail, but also reduce one of the more important hydrologic inputs in a region with water-dependent agriculture as its economic foundation (Smith et al. 2001; Hitchens and Brooks 2013; USGCRP 2018).

This study provided an initial set of perspectives on how the climatology of supercells may change in the CONUS during the twenty-first century. Our non-PGW approach permitted two future views—intermediate and pessimistic—on how changes in fundamental SCS ingredients and the general circulation may affect relatively long-lived, robust, cyclonic supercell populations. As stated, additional implicit and explicit research is required to improve our understanding of how ACC is affecting, and will affect, SCSs. These efforts should employ an ensemble modeling approach as computing and storage resources advance, as well as artificial intelligence methods to distill findings from voluminous simulation datasets. Indeed, our effort herein should be considered nascent, if limited, due to the computation, storage, and processing required to generate results using this simulation framework. There is considerable need for future work using multiple GCM inputs, both PGW and non-PGW approaches, additional RCP and/or shared socioeconomic pathways, use of multiple model cores, microphysics, and other parameterization schemes, and stochastic perturbations to initial model states to provide a more robust set of future climate solutions, as well as appreciate model biases and sensitivities (Gensini 2021). Further, the number of years we simulated was relatively small, but is equivalent to existing and ongoing dynamical downscaling efforts at this resolution. As computational and storage capabilities improve, simulations assessing the decades preceding the end of the twenty-first century are needed as many stakeholders are concerned—and, understandably so—with more imminent changes. Additional implicit efforts (cf. summaries provided by Brooks 2013; Tippett et al. 2015; Allen 2018; Raupach et al. 2021; Gensini 2021) examining fundamental SCS ingredients, and their overlap, is needed to help uncover the reasoning behind the trends this and other implicit studies are uncovering in simulated convective elements and their proxy hazards. Finally, integrating our new knowledge of how SCS risk will shift with the dynamic human-built environment exposure and vulnerability landscape is essential to understand the future of societal impacts from SCSs (e.g., Strader et al. 2017a,b). A community effort will be required to satisfy these immense research needs (Giorgi and Gutowski 2015; Kendon et al. 2021; Lucas-Picher et al. 2021; Takayabu et al. 2022; Giorgi et al. 2022) so that we can inform policy makers, weather-sensitive economic sectors, and the multiple publics that stand to be affected by SCSs.

Acknowledgments. This research was supported by the National Science Foundation Awards 1637225 and 1800582. The authors acknowledge high-performance computing support from Cheyenne (doi:10.5065/D6RX99HX) provided by NCAR's Computational and Information Systems Laboratory, sponsored by the National Science Foundation. We also acknowledge and thank Dr. Michael Papka (NIU/ANL) for data storage and postprocessing assistance. This research used resources of the Argonne Leadership Computing Facility, which is a DOE Office of Science User Facility supported under Contract DE-AC02-06CH11357. We thank the reviewers and editor for their feedback.

Data availability statement. In the spirit of reproducibility, if an email request is made to the authors, we will make available data and materials necessary to interested researchers for duplication and verification of results herein. WRF-BCC simulation output is available in netCDF format and stored on NCAR and/or Argonne systems. We request that anyone interested in using the WRF-BCC output contact coauthor Gensini (vgensini@niu.edu) for information on how to access the data, including any collaboration.

References

Allen, J. T., 2018: Climate change and severe thunderstorms. *Oxford Research Encyclopedia of Climate Science*, Oxford University Press, https://doi.org/10.1093/acrefore/9780190228620.013.62.

Anderson-Frey, A. K., and H. Brooks, 2019: Tornado fatalities: An environmental perspective. *Wea. Forecasting*, **34**, 1999–2015, https://doi.org/10.1175/WAF-D-19-0119.1.

Ashley, W. S., 2007: Spatial and temporal analysis of tornado fatalities in the United States: 1880–2005. *Wea. Forecasting*, **22**, 1214–1228, https://doi.org/10.1175/2007WAF2007004.1.

——, and S. M. Strader, 2016: Recipe for disaster: How the dynamic ingredients of risk and exposure are changing the tornado disaster landscape. *Bull. Amer. Meteor. Soc.*, **97**, 767–786, https://doi.org/10.1175/BAMS-D-15-00150.1.

——, A. J. Krmenec, and R. Schwantes, 2008: Vulnerability due to nocturnal tornadoes. *Wea. Forecasting*, **23**, 795–807, https://doi.org/10.1175/2008WAF2222132.1.

——, A. M. Haberlie, and J. Strohm, 2019: A climatology of quasi-linear convective systems and their hazards in the United States. *Wea. Forecasting*, **34**, 1605–1631, https://doi.org/10.1175/WAF-D-19-0014.1.

Brimelow, J. C., W. R. Burrows, and J. M. Hanesiak, 2017: The changing hail threat over North America in response to anthropogenic climate change. *Nat. Climate Change*, **7**, 516–522, https://doi.org/10.1038/nclimate3321.

Brooks, H. E., 2013: Severe thunderstorms and climate change. *Atmos. Res.*, **123**, 129–138, https://doi.org/10.1016/j.atmosres.2012.04.002.

——, and Coauthors, 2019: A century of progress in severe convective storm research and forecasting. *A Century of Progress in Atmospheric and Related Sciences: Celebrating the American Meteorological Society Centennial*, *Meteor. Monogr.*, No. 59, Amer. Meteor. Soc., https://doi.org/10.1175/AMSMONOGRAPHS-D-18-0026.1.

Browning, K. A., 1964: Airflow and precipitation trajectories within severe local storms which travel to the right of the winds. *J. Atmos. Sci.*, **21**, 634–639, https://doi.org/10.1175/1520-0469(1964)021<0634:AAPTWS>2.0.CO;2.

Bruyère, C. L., and Coauthors, 2014: Bias corrections of global models for regional climate simulations of high-impact weather. *Climate Dyn.*, **43**, 1847–1856, https://doi.org/10.1007/s00382-013-2011-6.

——, A. J. Monaghan, D. F. Steinhoff, and D. Yates, 2015: Bias-corrected CMIP5 CESM data in WRF/MPAS intermediate file format. NCAR Tech. Note NCAR/TN-515+STR, 27 pp., https://doi.org/10.5065/D6445JJ7.

Bunkers, M. J., B. A. Klimowski, J. W. Zeitler, R. L. Thompson, and M. L. Weisman, 2000: Predicting supercell motion using a new hodograph technique. *Wea. Forecasting*, **15**, 61–79, https://doi.org/10.1175/1520-0434(2000)015<0061:PSMUAN>2.0.CO;2.

——, M. R. Hjelmfelt, and P. L. Smith, 2006: An observational examination of long-lived supercells. Part I: Characteristics, evolution, and demise. *Wea. Forecasting*, **21**, 673–688, https://doi.org/10.1175/WAF949.1.

Burgess, D. W., V. T. Wood, and R. A. Brown, 1982: Mesocyclone evolution statistics. Preprints, *12th Conf. on Severe Local Storms*, San Antonio, TX, Amer. Meteor. Soc., 422–424.

Chen, J., and P. Kumar, 2002: Role of terrestrial hydrologic memory in modulating ENSO impacts in North America. *J. Climate*, **15**, 3569–3585, https://doi.org/10.1175/1520-0442(2003)015<3569:ROTHMI>2.0.CO;2.

Childs, S. J., R. S. Schumacher, and J. T. Allen, 2018: Cold-season tornadoes: Climatological and meteorological insights. *Wea. Forecasting*, **33**, 671–691, https://doi.org/10.1175/WAF-D-17-0120.1.

Christensen, J. H., F. Boberg, O. B. Christensen, and P. Lucas-Picher, 2008: On the need for bias correction of regional climate change projections of temperature and precipitation. *Geophys. Res. Lett.*, **35**, L20709, https://doi.org/10.1029/2008GL035694.

Christian, J., K. Christian, and J. B. Basara, 2015: Drought and pluvial dipole events within the Great Plains of the United States. *J. Appl. Meteor. Climatol.*, **54**, 1886–1898, https://doi.org/10.1175/JAMC-D-15-0002.1.

Clark, A. J., J. S. Kain, P. T. Marsh, J. Correia Jr., M. Xue, and F. Kong, 2012: Forecasting tornado pathlengths using a three-dimensional object identification algorithm applied to convection-allowing forecasts. *Wea. Forecasting*, **27**, 1090–1113, https://doi.org/10.1175/WAF-D-11-00147.1.

——, and Coauthors, 2013: Tornado pathlength forecasts from 2010 to 2011 using ensemble updraft helicity. *Wea. Forecasting*, **28**, 387–407, https://doi.org/10.1175/WAF-D-12-00038.1.

Daly, C., R. P. Neilson, and D. L. Phillips, 1994: A statistical–topographic model for mapping climatological precipitation over mountainous terrain. *J. Appl. Meteor. Climatol.*, **33**, 140–158, https://doi.org/10.1175/1520-0450(1994)033<0140:ASTMFM>2.0.CO;2.

Davenport, C. E., 2021: Environmental evolution of long-lived supercell thunderstorms in the Great Plains. *Wea. Forecasting*, **36**, 2187–2209, https://doi.org/10.1175/WAF-D-21-0042.1.

Davis, J. M., and M. D. Parker, 2014: Radar climatology of tornadic and nontornadic vortices in high-shear, low-CAPE environments in the mid-Atlantic and southeastern United States. *Wea. Forecasting*, **29**, 828–853, https://doi.org/10.1175/WAF-D-13-00127.1.

Dee, D. P., and Coauthors, 2011: The ERA-Interim reanalysis: Configuration and performance of the data assimilation system. *Quart. J. Roy. Meteor. Soc.*, **137**, 553–597, https://doi.org/10.1002/qj.828.

Diffenbaugh, N. S., M. Scherer, and R. J. Trapp, 2013: Robust increases in severe thunderstorm environments in response to greenhouse forcing. *Proc. Natl. Acad. Sci. USA*, **110**, 16 361–16 366, https://doi.org/10.1073/pnas.1307758110.

Doswell, C. A., III, 2001: Severe convective storms—An overview. *Severe Convective Storms*, *Meteor. Monogr.*, No. 50, Amer. Meteor. Soc., 1–26, https://doi.org/10.1175/0065-9401-28.50.1.

Duda, J. D., and W. A. Gallus Jr., 2010: Spring and summer Midwestern severe weather reports in supercells compared to other morphologies. *Wea. Forecasting*, **25**, 190–206, https://doi.org/10.1175/2009WAF2222338.1.

Edwards, R., A. R. Dean, R. L. Thompson, and B. T. Smith, 2012: Convective modes for significant severe thunderstorms in the contiguous United States. Part III: Tropical cyclone tornadoes. *Wea. Forecasting*, **27**, 1507–1519, https://doi.org/10.1175/WAF-D-11-00117.1.

Flournoy, M. D., and M. C. Coniglio, 2019: Origins of vorticity in a simulated tornadic mesovortex observed during PECAN on 6 July 2015. *Mon. Wea. Rev.*, **147**, 107–134, https://doi.org/10.1175/MWR-D-18-0221.1.

Gagne, D. J., II, A. McGovern, S. E. Haupt, R. A. Sobash, J. K. Williams, and M. Xue, 2017: Storm-based probabilistic hail forecasting with machine learning applied to convection-allowing ensembles. *Wea. Forecasting*, **32**, 1819–1840, https://doi.org/10.1175/WAF-D-17-0010.1.

Gallo, B. T., A. J. Clark, and S. R. Dembek, 2016: Forecasting tornadoes using convection-permitting ensembles. *Wea. Forecasting*, **31**, 273–295, https://doi.org/10.1175/WAF-D-15-0134.1.

Gensini, V. A., 2021: Severe convective storms in a changing climate. *Climate Change and Extreme Events*, A. Fares, Ed., Springer, 39–56, https://doi.org/10.1016/C2019-0-04922-9.

——, and W. S. Ashley, 2011: Climatology of potentially severe convective environments from North American regional reanalysis. *Electron. J. Severe Storms Meteor.*, **6** (8), https://ejssm.org/archives/wp-content/uploads/2021/09/vol6-8.pdf.

——, and T. L. Mote, 2014: Estimations of hazardous convective weather in the United States using dynamical downscaling. *J. Climate*, **27**, 6581–6589, https://doi.org/10.1175/JCLI-D-13-00777.1.

——, and ——, 2015: Downscaled estimates of late 21st century severe weather from CCSM3. *Climatic Change*, **129**, 307–321, https://doi.org/10.1007/s10584-014-1320-z.

——, and H. E. Brooks, 2018: Spatial trends in United States tornado frequency. *npj Climate Atmos. Sci.*, **1**, 38, https://doi.org/10.1038/s41612-018-0048-2.

——, and M. K. Tippett, 2019: Global Ensemble Forecast System (GEFS) predictions of days 1–15 U.S. tornado and hail frequencies. *Geophys. Res. Lett.*, **46**, 2922–2930, https://doi.org/10.1029/2018GL081724.

——, C. A. Ramseyer, and T. L. Mote, 2014: Future convective environments using NARCCAP. *Int. J. Climatol.*, **34**, 1699–1705, https://doi.org/10.1002/joc.3769.

——, A. M. Haberlie, and W. S. Ashley, 2022: Convection-permitting simulations of historical and possible future climate over the contiguous United States. *Climate Dyn.*, https://doi.org/10.1007/s00382-022-06306-0, in press.

Giorgi, F., and L. Mearns, 1999: Introduction to special section: Regional climate modeling revisited. *J. Geophys. Res*., **104**, 6335–6352, https://doi.org/10.1029/98JD02072.

——, and W. J. Gutowski Jr., 2015: Regional dynamical downscaling and the CORDEX initiative. *Annu. Rev. Environ. Resour.*, **40**, 467–490, https://doi.org/10.1146/annurev-environ-102014-021217.

——, and Coauthors, 2022: The CORDEX-CORE EXP-I initiative: Description and highlight results from the initial analysis. *Bull. Amer. Meteor. Soc.*, **103**, E293–E310, https://doi.org/10.1175/BAMS-D-21-0119.1.

Glazer, R. H., J. Torres-Alavez, E. Coppola, F. Giorgi, S. Das, M. Ashfaq, and T. Sines, 2021: Projected changes to severe thunderstorm environments as a result of twenty-first century warming from RegCM CORDEX-CORE simulations. *Climate Dyn.*, **57**, 1595–1613, https://doi.org/10.1007/s00382-020-05439-4.

Gropp, M. E., and C. E. Davenport, 2021: Python-based supercell tracking for coarse temporal and spatial resolution numerical model simulations. *J. Atmos. Oceanic Technol.*, **38**, 1551–1559, https://doi.org/10.1175/JTECH-D-20-0122.1.

Haberlie, A. M., and W. S. Ashley, 2018: A method for identifying midlatitude mesoscale convective systems in radar mosaics. Part II: Tracking. *J. Appl. Meteor. Climatol.*, **57**, 1599–1621, https://doi.org/10.1175/JAMC-D-17-0294.1.

——, and ——, 2019: Climatological representation of mesoscale convective systems in a dynamically downscaled climate simulation. *Int. J. Climatol.*, **39**, 1144–1153, https://doi.org/10.1002/joc.5880.

——, ——, C. M. Battisto, and V. A. Gensini, 2022: Thunderstorm activity under intermediate and extreme climate change scenarios. *Geophys. Res. Lett.*, **49**, e2022GL098779, https://doi.org/10.1029/2022GL098779.

Hitchens, N. M., and H. E. Brooks, 2013: Preliminary investigation of the contribution of supercell thunderstorms to the climatology of heavy and extreme precipitation in the United States. *Atmos. Res.*, **123**, 206–210, https://doi.org/10.1016/j.atmosres.2012.06.023.

Hocker, J. E., and J. B. Basara, 2008: A geographic information systems–based analysis of supercells across Oklahoma from 1994 to 2003. *J. Appl. Meteor. Climatol.*, **47**, 1518–1538, https://doi.org/10.1175/2007JAMC1673.1.

Hoogewind, K. A., M. E. Baldwin, and R. J. Trapp, 2017: The impact of climate change on hazardous convective weather in the United States: Insight from high-resolution dynamical downscaling. *J. Climate*, **30**, 10081–10100, https://doi.org/10.1175/JCLI-D-16-0885.1.

Houze, R. A., Jr., 2018: 100 years of research on mesoscale convective systems. *A Century of Progress in Atmospheric and Related Sciences: Celebrating the American Meteorological Society Centennial*, *Meteor. Monogr.*, No. 59, Amer. Meteor. Soc., https://doi.org/10.1175/AMSMONOGRAPHS-D-18-0001.1.

Hua, Z., and A. K. Anderson-Frey, 2022: Self-organizing maps for the classification of spatial and temporal variability of tornado-favorable parameters. *Mon. Wea. Rev.*, **150**, 393–407, https://doi.org/10.1175/MWR-D-21-0168.1.

Ines, A. V., and J. W. Hansen, 2006: Bias correction of daily GCM rainfall for crop simulation studies. *Agric. For. Meteor.*, **138**, 44–53, https://doi.org/10.1016/j.agrformet.2006.03.009.

IPCC, 2014: *Climate Change 2014: Synthesis Report.* R. K. Pachauri and L. A. Meyer, Eds., IPCC, 151 pp., www.ipcc.ch/report/ar5/syr/.

——, 2021: *Climate Change 2021: The Physical Science Basis.* V. Masson-Delmotte et al., Eds., Cambridge University Press, 2409 pp., www.ipcc.ch/report/ar6/wg1/.

Kain, J. S., and Coauthors, 2008: Some practical considerations regarding horizontal resolution in the first generation of operational convection-allowing NWP. *Wea. Forecasting*, **23**, 931–952, https://doi.org/10.1175/WAF2007106.1.

Kendon, E. J., A. F. Prein, C. A. Senior, and A. Stirling, 2021: Challenges and outlook for convection-permitting climate modelling. *Philos. Trans. Roy. Soc.*, **379A**, 20190547, https://doi.org/10.1098/rsta.2019.0547.

Krocak, M. J., and H. E. Brooks, 2018: Climatological estimates of hourly tornado probability for the United States. *Wea. Forecasting*, **33**, 59–69, https://doi.org/10.1175/WAF-D-17-0123.1.

——, M. D. Flournoy, and H. E. Brooks, 2021: Examining subdaily tornado warning performance and associated environmental characteristics. *Wea. Forecasting*, **36**, 1779–1784, https://doi.org/10.1175/WAF-D-21-0097.1.

Kunkel, K. E., and Coauthors, 2013: Monitoring and understanding trends in extreme storms: State of knowledge. *Bull. Amer. Meteor. Soc.*, **94**, 499–514, https://doi.org/10.1175/BAMS-D-11-00262.1.

Lakshmanan, V., M. Miller, and T. Smith, 2013: Quality control of accumulated fields by applying spatial and temporal constraints. *J. Atmos. Oceanic Technol.*, **30**, 745–758, https://doi.org/10.1175/JTECH-D-12-00128.1.

Lepore, C., R. Abernathey, N. Henderson, J. T. Allen, and M. K. Tippett, 2021: Future global convective environments in CMIP6 models. *Earth's Future*, **9**, e2021EF002277, https://doi.org/10.1029/2021EF002277.

Liu, C., and Coauthors, 2016: Continental-scale convection-permitting modeling of the current and future climate of North America. *Climate Dyn.*, **49**, 71–95, https://doi.org/10.1007/s00382-016-3327-9.

Lucas-Picher, P., and Coauthors, 2021: Convection-permitting modeling with regional climate models: Latest developments and next steps. *Wiley Interdiscip. Rev.: Climate Change*, **12**, e731, https://doi.org/10.1002/wcc.731.

Marion, G. R., and R. Trapp, 2019: The dynamical coupling of convective updrafts, downdrafts, and cold pools in simulated supercell thunderstorms. *J. Geophys. Res. Atmos.*, **124**, 664–683, https://doi.org/10.1029/2018JD029055.

Markowski, P. M., 2020: What is the intrinsic predictability of tornadic supercell thunderstorms? *Mon. Wea. Rev.*, **148**, 3157–3180, https://doi.org/10.1175/MWR-D-20-0076.1.

——, and Y. Richardson, 2010: *Mesoscale Meteorology in Midlatitudes.* Wiley-Blackwell, 432 pp., https://doi.org/10.1002/9780470682104.

Mason, L. R., K. N. Ellis, B. Winchester, and S. Schexnayder, 2018: Tornado warnings at night: Who gets the message? *Wea. Climate Soc.*, **10**, 561–568, https://doi.org/10.1175/WCAS-D-17-0114.1.

Miguez-Macho, G., G. L. Stenchikov, and A. Robock, 2004: Spectral nudging to eliminate the effects of domain position and geometry in regional climate model simulations. *J. Geophys. Res.*, **109**, D13104, https://doi.org/10.1029/2003JD004495.

Molina, M. J., D. J. Gagne, and A. F. Prein, 2021: A benchmark to test generalization capabilities of deep learning methods to classify severe convective storms in a changing climate. *Earth Space Sci.*, **8**, e2020EA001490, https://doi.org/10.1029/2020EA001490.

Morin, M. J., and M. D. Parker, 2011: A numerical investigation of supercells in landfalling tropical cyclones. *Geophys. Res. Lett*., **38**, L10801, https://doi.org/10.1029/2011GL047448.

Moss, R. H., and Coauthors, 2010: The next generation of scenarios for climate change research and assessment. *Nature*, **463**, 747–756, https://doi.org/10.1038/nature08823.

NAS, 2016: *Attribution of Extreme Weather Events in the Context of Climate Change.* National Academies Press, 186 pp., https://doi.org/10.17226/21852.

Naylor, J., M. S. Gilmore, R. L. Thompson, R. Edwards, and R. B. Wilhelmson, 2012: Comparison of objective supercell identification techniques using an idealized cloud model. *Mon. Wea. Rev.*, **140**, 2090–2102, https://doi.org/10.1175/MWR-D-11-00209.1.

Pilguj, N., M. Taszarek, J. T. Allen, and K. Hoogewind, 2022: Are trends in convective parameters over the United States and Europe consistent between reanalyses and observations? *J. Climate*, **35**, 3605–3626, https://doi.org/10.1175/JCLI-D-21-0135.1.

Potvin, C. K., and M. L. Flora, 2015: Sensitivity of idealized supercell simulations to horizontal grid spacing: Implications for Warn-on-Forecast. *Mon. Wea. Rev.*, **143**, 2998–3024, https://doi.org/10.1175/MWR-D-14-00416.1.

Prein, A. F., and Coauthors, 2015: A review on regional convection-permitting climate modeling: Demonstrations, prospects, and challenges. *Rev. Geophys.*, **53**, 323–361, https://doi.org/10.1002/2014RG000475.

Rasmussen, K. L., A. F. Prein, R. M. Rasmussen, K. Ikeda, and C. Liu, 2017: Changes in the convective population and thermodynamic environments in convection-permitting regional climate simulations over the United States. *Climate Dyn.*, **55**, 383–408, https://doi.org/10.1007/s00382-017-4000-7.

Raupach, T. H., and Coauthors, 2021: The effects of climate change on hailstorms. *Nat. Rev. Earth Environ.*, **2**, 213–226, https://doi.org/10.1038/s43017-020-00133-9.

Robinson, E. D., R. J. Trapp, and M. E. Baldwin, 2013: The geospatial and temporal distributions of severe thunderstorms from high-resolution dynamical downscaling. *J. Appl. Meteor. Climatol.*, **52**, 2147–2161, https://doi.org/10.1175/JAMC-D-12-0131.1.

Rossum, S., and S. Lavin, 2000: Where are the Great Plains? A cartographic analysis. *Prof. Geogr.*, **52**, 543–552, https://doi.org/10.1111/0033-0124.00245.

Schenkman, A. D., and M. Xue, 2016: Bow-echo mesovortices: A review. *Atmos. Res.*, **170**, 1–13, https://doi.org/10.1016/j.atmosres.2015.11.003.

Schoen, J., and W. S. Ashley, 2011: A climatology of fatal convective wind events by storm type. *Wea. Forecasting*, **26**, 109–121, https://doi.org/10.1175/2010WAF2222428.1.

Seeley, J. T., and D. M. Romps, 2015: The effect of global warming on severe thunderstorms in the United States. *J. Climate*, **28**, 2443–2458, https://doi.org/10.1175/JCLI-D-14-00382.1.

Sherburn, K. D., and M. D. Parker, 2014: Climatology and ingredients of significant severe convection in high-shear, low-CAPE environments. *Wea. Forecasting*, **29**, 854–877, https://doi.org/10.1175/WAF-D-13-00041.1.

Skamarock, W. C., and Coauthors, 2021: A description of the Advanced Research WRF Model version 4.3. NCAR Tech. Note NCAR/TN-556+STR, 165 pp., https://doi.org/10.5065/1dfh-6p97.

Smith, B. T., R. L. Thompson, J. S. Grams, C. Broyles, and H. E. Brooks, 2012: Convective modes for significant severe thunderstorms in the contiguous United States. Part I: Storm classification and climatology. *Wea. Forecasting*, **27**, 1114–1135, https://doi.org/10.1175/WAF-D-11-00115.1.

Smith, J. A., M. L. Baeck, Y. Zhang, and C. A. Doswell III, 2001: Extreme rainfall and flooding from supercell thunderstorms. *J. Hydrometeor.*, **2**, 469–489, https://doi.org/10.1175/1525-7541(2001)002<0469:ERAFFS>2.0.CO;2.

Sobash, R. A., and J. S. Kain, 2017: Seasonal variations in severe weather forecast skill in an experimental convection-allowing model. *Wea. Forecasting*, **32**, 1885–1902, https://doi.org/10.1175/WAF-D-17-0043.1.

——, ——, D. R. Bright, A. R. Dean, M. C. Coniglio, and S. J. Weiss, 2011: Probabilistic forecast guidance for severe thunderstorms based on the identification of extreme phenomena in convection-allowing model forecasts. *Wea. Forecasting*, **26**, 714–728, https://doi.org/10.1175/WAF-D-10-05046.1.

——, C. S. Schwartz, G. S. Romine, K. R. Fossell, and M. L. Weisman, 2016a: Severe weather prediction using storm surrogates from an ensemble forecasting system. *Wea. Forecasting*, **31**, 255–271, https://doi.org/10.1175/WAF-D-15-0138.1.

——, G. S. Romine, C. S. Schwartz, D. J. Gagne II, and M. L. Weisman, 2016b: Explicit forecasts of low-level rotation from convection-allowing models for next-day tornado prediction. *Wea. Forecasting*, **31**, 1591–1614, https://doi.org/10.1175/WAF-D-16-0073.1.

Strader, S. M., W. S. Ashley, T. J. Pingel, and A. J. Krmenec, 2017a: Projected 21st century changes in tornado exposure, risk, and disaster potential. *Climatic Change*, **141**, 301–313, https://doi.org/10.1007/s10584-017-1905-4.

——, ——, ——, and ——, 2017b: Observed and projected changes in United States tornado exposure. *Wea. Climate Soc.*, **9**, 109–123, https://doi.org/10.1175/WCAS-D-16-0041.1.

——, A. Haberlie, and A. Loitz, 2021: Assessment of NWS county warning area tornado risk, exposure, and vulnerability. *Wea. Climate Soc.*, **12**, 189–209, https://doi.org/10.1175/WCAS-D-20-0107.1.

——, W. Ashley, A. M. Haberlie, and K. Kaminski, 2022: Revisiting U.S. nocturnal tornado vulnerability and its influence on tornado impacts. *Wea. Climate Soc.*, **14**, 1147–1163, https://doi.org/10.1175/WCAS-D-22-0020.1.

Takayabu, I., and Coauthors, 2022: Convection-permitting models for climate research. *Bull. Amer. Meteor. Soc.*, **103**, E77–E82, https://doi.org/10.1175/BAMS-D-21-0043.1.

Taszarek, M., J. T. Allen, T. Púčik, K. Hoogewind, and H. E. Brooks, 2020: Severe convective storms across Europe and the United States. Part II: ERA5 environments associated with lightning, large hail, severe wind, and tornadoes. *J. Climate*, **33**, 10 263–10 286, https://doi.org/10.1175/JCLI-D-20-0346.1.

——, ——, H. E. Brooks, N. Pilguj, and B. Czernecki, 2021: Differing trends in United States and European severe thunderstorm environments in a warming climate. *Bull. Amer. Meteor. Soc.*, **102**, E296–E322, https://doi.org/10.1175/BAMS-D-20-0004.1.

Thompson, R. L., R. Edwards, J. A. Hart, K. L. Elmore, and P. Markowski, 2003: Close proximity soundings within supercell environments obtained from the Rapid Update Cycle. *Wea. Forecasting*, **18**, 1243–1261, https://doi.org/10.1175/1520-0434(2003)018<1243:CPSWSE>2.0.CO;2.

——, B. T. Smith, J. S. Grams, A. R. Dean, and C. Broyles, 2012: Convective modes for significant severe thunderstorms in the contiguous United States. Part II: Supercell and QLCS tornado environments. *Wea. Forecasting*, **27**, 1136–1154, https://doi.org/10.1175/WAF-D-11-00116.1.

Tippett, M. K., J. T. Allen, V. A. Gensini, and H. E. Brooks, 2015: Climate and hazardous convective weather. *Curr. Climate Change Rep.*, **1**, 60–73, https://doi.org/10.1007/s40641-015-0006-6.

Trapp, R. J., and M. L. Weisman, 2003: Low-level mesovortices within squall lines and bow echoes. Part II: Their genesis and implications. *Mon. Wea. Rev.*, **131**, 2804–2823, https://doi.org/10.1175/1520-0493(2003)131<2804:LMWSLA>2.0.CO;2.

——, and K. A. Hoogewind, 2016: The realization of extreme tornadic storm events under future anthropogenic climate change. *J. Climate*, **29**, 5251–5265, https://doi.org/10.1175/JCLI-D-15-0623.1.

——, N. S. Diffenbaugh, H. E. Brooks, M. E. Baldwin, E. D. Robinson, and J. S. Pal, 2007: Changes in severe thunderstorm environment frequency during the 21st century caused by anthropogenically enhanced global radiative forcing. *Proc. Natl. Acad. Sci. USA*, **104**, 19 719–19 723, https://doi.org/10.1073/pnas.0705494104.

——, ——, and A. Gluhovsky, 2009: Transient response of severe thunderstorm forcing to elevated greenhouse gas concentrations. *Geophys. Res. Lett.*, **36**, L01703, https://doi.org/10.1029/2008GL036203.

——, E. D. Robinson, M. E. Baldwin, N. S. Diffenbaugh, and B. R. J. Schwedler, 2011: Regional climate of hazardous convective weather through high-resolution dynamical downscaling. *Climate Dyn.*, **37**, 677–688, https://doi.org/10.1007/s00382-010-0826-y.

——, K. A. Hoogewind, and S. Lasher-Trapp, 2019: Future changes in hail occurrence in the United States determined through convection-permitting dynamical downscaling. *J. Climate*, **32**, 5493–5509, https://doi.org/10.1175/JCLI-D-18-0740.1.

——, M. J. Woods, S. G. Lasher-Trapp, and M. A. Grover, 2021: Alternative implementations of the "pseudo-global-warming" methodology for event-based simulations. *J. Geophys. Res. Atmos.*, **126**, e2021JD035017, https://doi.org/10.1029/2021JD035017.

USGCRP, 2018: *Impacts, Risks, and Adaptation in the United States: Fourth National Climate Assessment.* D. R. Reidmiller, Ed., Vol. II, U.S. Global Change Research Program, 1515 pp., https://doi.org/10.7930/NCA4.2018.

Weisman, M. L., and R. J. Trapp, 2003: Low-level mesovortices within squall lines and bow echoes. Part I: Overview and dependence on environmental shear. *Mon. Wea. Rev.*, **131**, 2779–2803, https://doi.org/10.1175/1520-0493(2003)131<2779:LMWSLA>2.0.CO;2.

Wood, V. T., R. A. Brown, and D. W. Burgess, 1996: Duration and movement of mesocyclones associated with southern Great Plains thunderstorms. *Mon. Wea. Rev.*, **124**, 97–101, https://doi.org/10.1175/1520-0493(1996)124<0097:DAMOMA>2.0.CO;2.